2022 NDIA MICHIGAN CHAPTER
GROUND VEHICLE SYSTEMS ENGINEERING
AND TECHNOLOGY SYMPOSIUM
ADVANCED MATERIALS & MANUFACTURING TECHNICAL SESSION
AUGUST 16-18, 2022 - NOVI, MICHIGAN

Microstructure analysis of TIG weld joints of Ni-based superalloys produced by Laser Powder Bed Fusion

Ole Geisen [1]*, Jan Bogner [1], Ebrahim Ghavampour[1], Vinzenz Müller[2], Katharina Eissing[3]

[1] Siemens Gas and Power GmbH & Co. KG, Berlin, Germany
[2] Fraunhofer Institute for Production Systems & Design Technology IPK, Berlin, Germany
[3] Advanced Manufacturing Lab, ETH Zurich, Zurich, Switzerland
* Correspondence: ole.geisen@siemens-energy.com

Abstract

The industrial use of laser powder-bed fusion (L-PBF) in turbomachinery is gaining momentum rendering the inspection and qualification of certain post-processing steps necessary. This includes fusion techniques that allow to print multiple parts separately to take advantage of e.g., various print orientations and join them subsequently. The main motivation of this study is to validate the tungsten inert gas (TIG) welding process of L-PBF manufactured parts using industrial specifications relevant for gas turbines to pave the way for the industrial production of modular build setups. For this, two commonly used nickel-based super alloys for high-temperature applications, Inconel 718 and Inconel 625 are chosen. Since their defect-free printability has been established widely, we focus on the suitability to be joined using TIG welding. The process is evaluated performing microstructural examination and mechanical tests in as built as well as heat-treated samples. The welds are assessed by applying a general weld qualification approach used at Siemens Energy - Gas and Power. It was found that both materials can be joined via TIG welding using standard weld parameters causing minimal defects. A solution annealing heat treatment before welding is not necessary for a positive outcome, but still recommended for Inconel 718.

---

1. Introduction

L-PBF is an Additive Manufacturing (AM) technology which, due to the achievable feature resolution and processability of high-performance materials, is suited for gas turbine applications. It is possible to produce L-PBF parts with similar mechanical and physical properties to those produced by conventional technologies such as casting. In addition, the technology allows for the manufacturing of highly complex and individualized components without the cost-intensive production of casting or forging molds for every design iteration. While the L-PBF technology comes with a lot of technical promises and opportunities, it still struggles to compete on an economical basis with already established production methods. Market studies have found that a drop in part production costs by a factor of ten is needed for the technology to become widely accepted in the industry.

Many L-PBF applications for gas turbines today focus on the hot-gas path, where complex internal cooling features are employed, to utilize the design freedom of the

technology. The use of L-PBF in rotating parts is still limited due to insufficient creep resistance of the materials available. While a common design approach in AM is to integrate multiple parts into one, subsequent joining is sometimes still required. The main reasons for using non-monolithic build-setups may be limitations of the build chamber size or avoiding support-structures, e.g., for internal structures, which may require specific build orientations for unique features of a part. In both cases a modular build strategy can be beneficial. However, this creates the need for an adequate joining process in the subsequent assembly. In turbomachinery, as in all quality-conscious industries, both the material properties and the post-processing technologies, such as welding and joining, need to be qualified according to specifications.

Nickel superalloys Inconel 625 (IN625) and Inconel 718 (IN718) are commonly used in a wide variety of applications in turbomachinery and aerospace due to their good corrosion resistance, excellent mechanical properties at elevated temperatures and weldability. It has been well established that these materials can be manufactured by L-PBF without defects. In general, most L-PBF parts require a post-processing heat treatment to reduce residual stresses or to obtain the required structural performance, for example via recrystallization (IN625) or precipitation hardening (IN718). Although the chemical composition of IN625 and IN718 powders for L-PBF is the same as that corresponding to cast ingots, the different boundary conditions in the production process, such as the extreme cooling rates of the melt pools, give rise to different microstructures and properties. Analyses on relevant techniques such as TIG welding of conventionally manufactured parts out of these materials are well established and available. However, no studies on TIG-welding of L-PBF components using industrial specifications relevant for gas turbines have been published to date. Thus, investigating whether the metallurgical differences associated to L-PBF production methods have an influence on the quality of TIG-welds is timely.

The aim of this work is to investigate the applicability of TIG welding to Ni-superalloy components fabricated by L-PBF methods. Two scenarios of interest for gas turbine use cases are investigated and compared in this study, namely welding in the as-built condition, or following a post-processing heat treatment. The first scenario has the potential to reduce the process chain complexity and is therefore interesting for industrialization. For both scenarios, the development of microstructure and the associated hardness were investigated on the cross-section areas of the weld seam.

System requirements for armored fighting vehicles (AFVs) are constantly evolving. Missions require vehicles that can provide a greater degree of protection and higher performance at reduced weight which strains the capabilities of conventional manufacturing methods. The potential benefits of additive to ground vehicles have been discussed at length elsewhere. When adopting an additive design, material selection becomes problematic. A lot of ferrous components in ground systems are fabricated from carbon and alloy steels. Oftentimes, these materials are not available or economical in powder form for additive which is focused on use of higher performance alloys utilized in energy generation, marine applications, and biomedical industries

As a result, when looking at development of additively manufactured components for AFVs, it is important for a designer to focus on the property requirements or end performance needs of a component rather than attempting to stay within existing material selection

guidelines. A list of some ferrous materials commonly used in AFV construction are listed below along with nearest equivalent products common to additive manufacturing.

			Room Temperature	
Product Form	Class or Type	Spec - ASTM	YS (KSI)	UTS (KSI)
Wrought	-	A36	36 min	58-80
	-	A588	42 min	63 min
	4130, Normalized	A322	60 typ	80 typ
	4130, HRC 28-32	A322	95 -100 approx.	130-140 approx.
Cast	105-85	A148	85 min	105 min
Additive Properties (LPBF)				
Industry Standard	Inco 625	F3056	40 min	70 min
	Inco 718	F3055	85 min	133 min

For higher strength applications, precipitation hardened stainless steels, maraging steels, or titanium alloys may also be relevant for AFV applications but will not be discussed in the scope of this document. In looking at replacement of structural steel and alloy steel product with maximum tensile strength near 100 ksi, Inconel 625 and 718 are readily available and well developed as material for additive manufacturing. By utilizing these materials which are not common to AFVs, new designs can enjoy economies of scale and supply chains already established by energy and biomedical sectors rather than attempting to establish new ones. Most commercially available powder bed fusion (PBF) systems from major manufacturers support these materials out-of-the-box and processing parameters are readily available from public sources when needed. This reduces the development time needed to design and manufacture a concept component for an AFV. (While offering increased performance in material strength and corrosion resistance)
Additionally, components on these systems tend to be large compared to those currently being fabricated additively. As such, joining of discrete printed sections to wrought product or other printed sections may be required and the properties of these joints must be considered to ensure proper design. Table 2 shows listings of commonly used steel welding consumables for AFVs and their comparison to similar requirements for conventional additive material selections.
The table below shows select welded property minimums for common ferrous materials and additive alternatives.

Weld Material	Specification	UTS
70S	AWS A5.18	70 min
100S	AWS A5.28	100 min
4130 (HRC 28 – 32)	-	130 – 140 approx.
Inconel 625	ASME BPVC IX	110 min

Given that Inconel 625 is readily arc weldable by a range of conventional processes and has a history of use in several accepted codes and standards, this material should be considered when engineering additive parts of AFVs.

2. Materials and Methods

Table 1. Chemical composition of Inconel 718

Chemical composition of IN718 in percent by weight						
Ni	Cr	Nb	Mo	Ti	Al	Co
50.0-55.0	17.0-21.0	4.75-5.5	2.8-3.3	0.65-1.15	0.2-0.8	≤ 1.0
Cu	C	Si, Mn	P, S	B	Fe	ρ $[g/cm^3]$
≤ 0.3	≤ 0.08	≤ 0.35	≤ 0.015	≤0.006	≤11.5	8.15

Table 2. Chemical composition of Inconel 625

Chemical composition of IN625 in percent by weight						
Ni	Cr	Nb+Ta	Mo	O	Ti, Al	Co
≥ 58.0	20.0-23.0	3.15-4.15	8.-10.0	≤ 0.03	≤ 0.4	≤ 1.0
Cu	C	Si, Mn	P, S	N	Fe	ρ $[g/cm^3]$
≤ 0.50	≤ 0.10	≤ 0.50	≤ 0.015	≤0.02	≤5.0	8.4

In this study, commercial IN718 powder from EOS GmbH (EOS Nickel Alloy IN718) and IN625 powder from LPW Technology Limited (LPW-625-AACP), both produced by gas atomization, were used. The chemical compositions are shown in Table 1 and Table 2, respectively. Both powder alloys contain fine-grained, spherical metal particles with properties suitable for L-PBF. The corresponding gaussian particle si distributions have a $d_{100} = 15 - 45\mu m$.

Table 3. Chemical composition of Thermanit 625

Chemical composition of Thermanit 625 in percent by weight						
C	Si	Cr	Mo	Ni	Nb	Fe
≤ 0.02	≤ 0.02	22.0	9.0	Rest	3.5	1

Table 4. Parameters for solution annealing heat treatment of IN718

	Program section	Process time [s]	Temperature [°C]	Heating/ cooling rate [°C/min]	Atmosphere
1	start	0	25		high vacuum
2	heating	6900	1175	10	high vacuum
3	storing	10500	1175		high vacuum
4	rapid cooling	11310	500	50	Argon
5	free cooling	20880	25		Argon

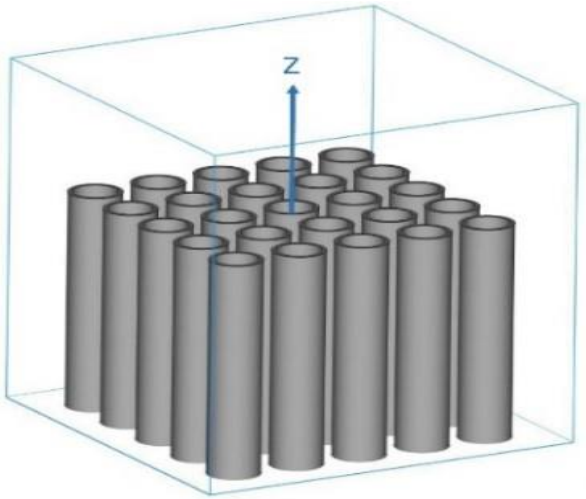

Figure 1. Welding procedure according to DIN EN ISO 9606-04 and welding positions according to DIN EN ISO 6947

Table 5. Parameters for solution annealing heat treatment of IN625

	Program section	Process time [s]	Temperature [°C]	Heating/ cooling rate [°C/min]	Atmosphere
1	start	0	25		high vacuum
2	heating	4776	980	12	high vacuum
3	storing	8376	980		high vacuum
4	rapid cooling	8952	500	50	Argon
5	free cooling	17640	25		Argon

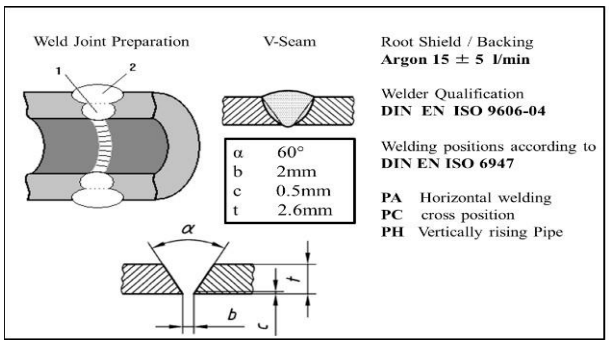

Figure 2. L-PBF build job setup of welding test specimens

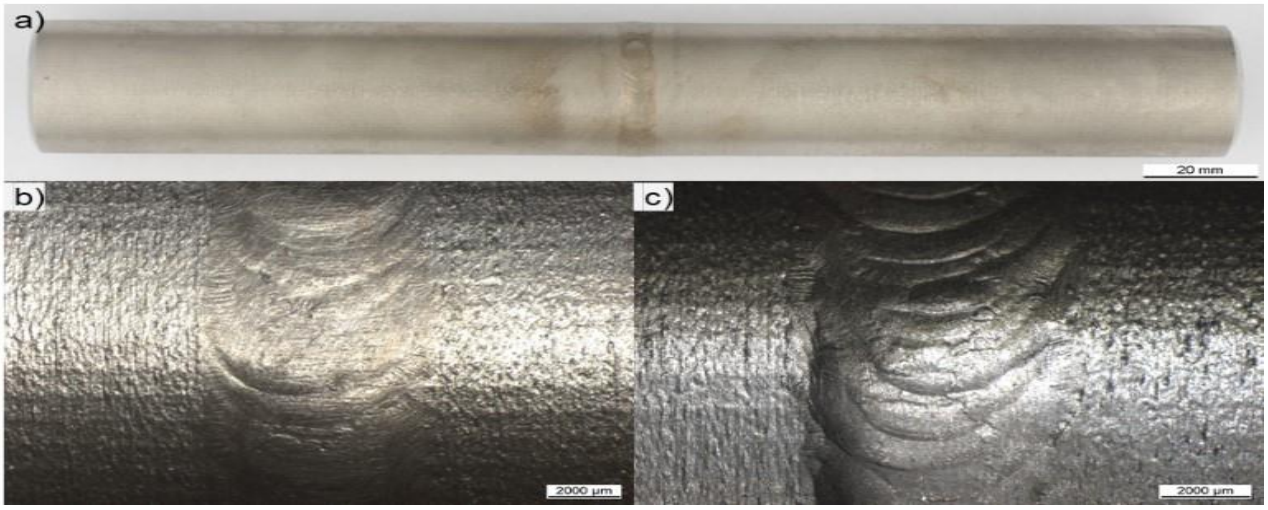

Figure 3. Two pipes TIG-welded together (a), Light microscopy photo (10x) of a weld seam of non-heat treated (b) and heat-treated IN718 (c).

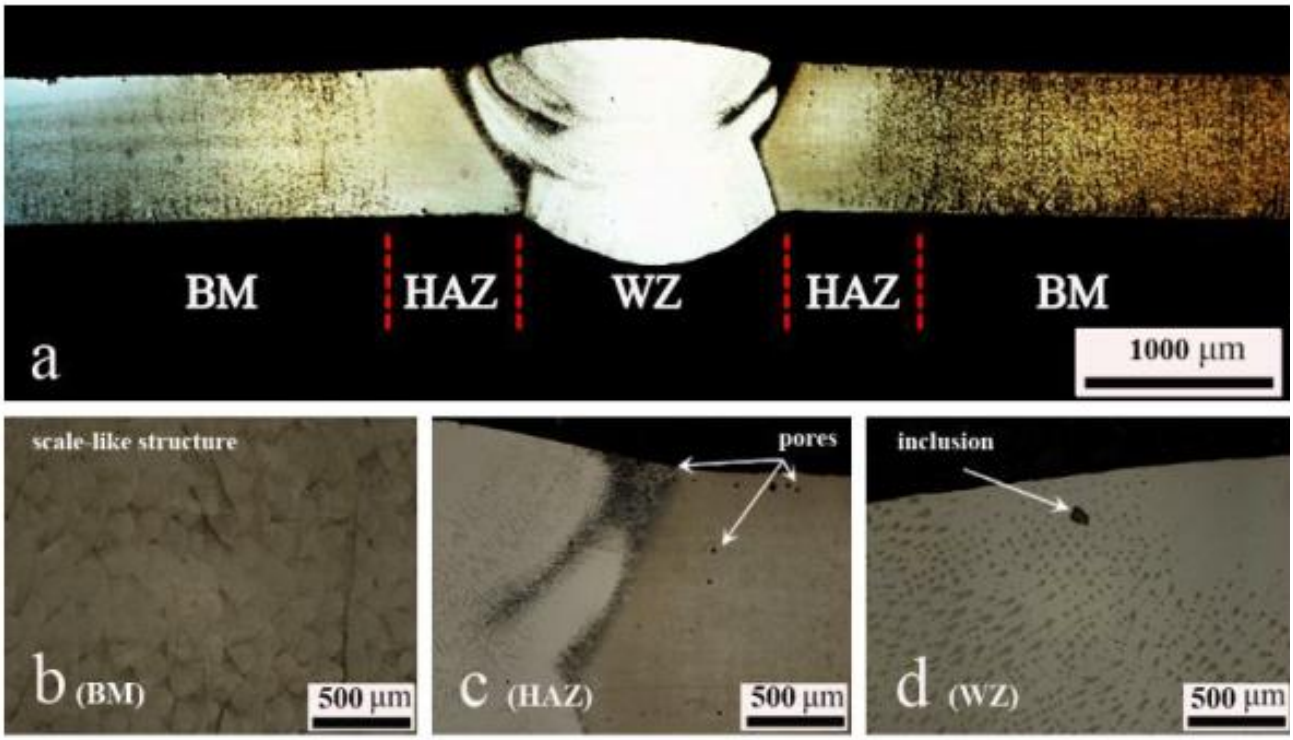

Figure 4. Light microscope images of cross sections of the IN718 specimen without heat treatment a) Overview b) Base material with typical flake structure c) Heat-affected zone with pores d) Weld seam with inclusion.

L-PBF manufacturing was carried out in an EOS M290 machine. The manufactured parts were pipes with a length of 100 mm, an outer diameter of 33.2 mm and a wall thickness of 1.6 mm. All specimens were printed with EOS' standard parameters for IN718 at a layer thickness of 40μm using argon as inert gas. The tubes were built vertically in multiple build jobs, as shown in Figure 1. Some L-PBF parts thus manufactured were additionally

solid solution treated to investigate the effect of annealing on the weldability. A detailed list of the heat treatment conditions is specified for IN718 in Table 4 and for IN625 in Table 5.

As built and heat-treated samples were then TIG welded in the following way. A turning operation was first carried out to produce a V-seam weld preparation with an opening angle of 60°. TIG-welding of the pipes was then conducted manually in two layers in a PA (horizontal), PC (cross) and PH (vertically rising pipe) position (as per DIN EN ISO 6947) while a gap of approximately 2 mm was left between the specimens. The welding procedure including the welding positions is shown in Figure 2. Thermanit 625 (or UTP A 6222 Mo) was used as filler metal for all specimens. The chemical composition is listed in Table 3.

The weld joints were first inspected visually and by light microscopy. Figure 3 shows an image of the welded tubes obtained using a digital camera (Fig. 3a) as well as optical macrographs of two welds performed in as-built (Fig. 3b) and heat-treated (Fig.3b) IN718. The cross sections were prepared with Kalling's 2 reagent to enhance the visibility of features under the bright field light microscopy. No major defects can be appreciated at this low magnification examination in either of the two materials investigated. The microstructure of the weld joints was also imaged by electron backscattered diffraction (EBSD) using a scanning electron microscope equipped with a CCD camera.

The presence of microstructural gradients in welds may lead to local variations of the hardness, which might reach levels that are detrimental for a component's life. In this study, the Vickers hardness was measured on a cross section of the welds according to DIN EN ISO 9015-1. Instead of the ten indentations required by the standard, 21 measurements were performed for a more detailed analysis.

3. Results and discussion

Figure 4 illustrates an Inconel 718 cut weld seam in the as-built condition. The structural differences between the base material (BM), the heat-affected zone (HAZ) and the weld zone (WZ) can be noted visually. As shown in 4b, melt pools can be clearly distinguished in the BM of the L-PBF manufactured pipes. Some pores can be seen close to the surface in the BM. However, melt pool boundaries are no longer visible in the HAZ, revealing the occurrence of microstructural changes because of welding (Fig.3c). Pores can also be found in the HAZ, close to the weld seam. The IN625 welds in the as-built condition exhibit a similar appearance at this magnification. welds in the as-built condition exhibit a similar appearance at this magnification.

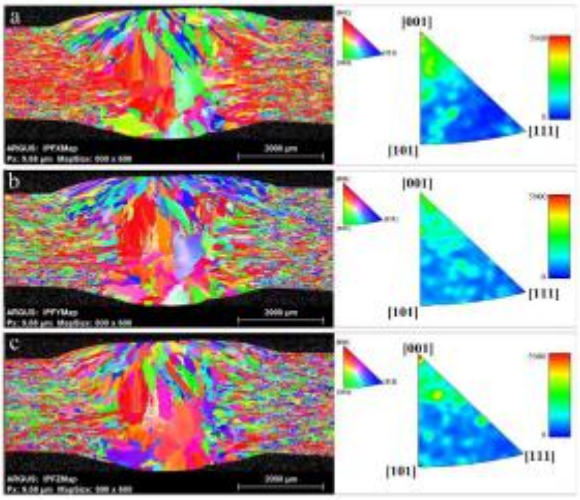

Figure 5. EBSD measurements of cross section of IN718 specimen without solution annealing heat treatment; a) IPFX map with inverse pole figure of X direction b) IPFY map with inverse pole figure of Y direction c) IPFZ Map with inverse pole figure of Z direction.

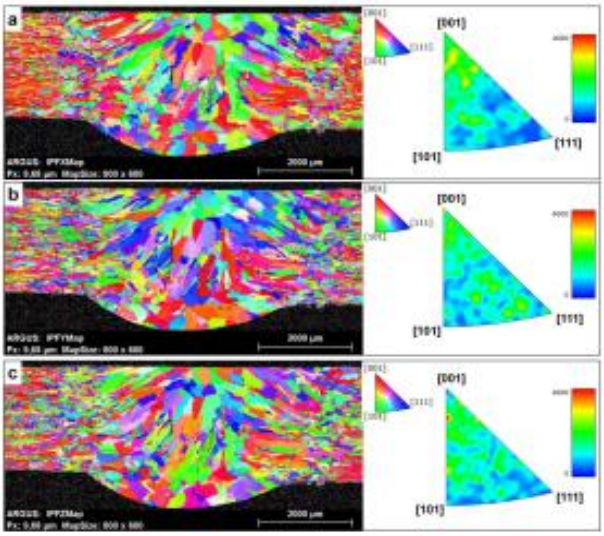

Figure 6. EBSD measurements of cross section of IN625 specimen without solution annealing heat treatment; a) IPFX map with inverse pole figure of X direction b) IPFY map with inverse pole figure of Y direction c) IPFZ Map with inverse pole figure of Z direction.

Figures 5 and 6 show the microstructure of the IN718 and IN625 welds, respectively, in the as-built condition. In both cases, EBSD inverse pole figure maps in three perpendicular directions are given. The horizontal direction in the map (X) is parallel to the building direction. The corresponding inverse pole figures are also included in these figures. The latter were determined for the entire area of the EBSD maps and accordingly indicate the crystallographic preferential orientations for all zones (BM, HAZ, WZ). It must be noted here that, since the grains in the WZ, especially those in the root layer, occupy a large volume, they have a large influence on the inverse pole figure. In both materials, the BM and HAZ are populated with grains that are elongated along the building direction, and possess a typical crystallographic texture, in which the building direction is mostly parallel to a direction, as is usually observed in L-PBF manufactured Ni superalloys. Overall, the grain size within the WZ is significantly larger than that of the BM and HAZ. The WZ is formed by two layers. The root layer consists mostly of equiaxed grains, while the grains at the top layer are elongated along the direction of thermal flow. Within the WZ, in the IN718 weld, the large grains at the root layer tend to orient with a direction parallel to all three perpendicular axes examined. In the IN625 alloy the grains at the root layer are, however, more randomly oriented, and slightly smaller in size.

Figure 7 depicts an IN718 cut weld seam in the heat-treated condition. At least visually, the difference between the BM (Fig.7b) and the HAZ (Fig.7c)) is much less pronounced for the heat-treated compared to the non- heat- treated pipes.

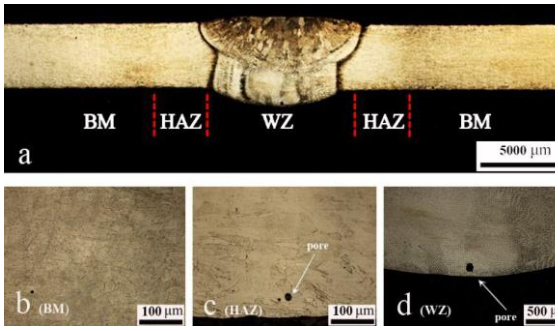

Figure 7. Light microscopic images of the cross sections etched with Kalling's 2 in brightfield for IN718 with heat treatment a) Overview; b) Base material c) Heat-affected zone with pore d) Weld seam with pore

The heat treatment of the BM caused a visible change in the components' texture. As shown in Fig. 7b, the scale-like surface-structure is no longer visible. Instead, a more homogenous structure can be seen. Some pores can still be found in the BM, in regions located near the surface. The IN625 welds in the heat-treated condition exhibit a similar appearance at this magnification. Figures 8 and 9 illustrate the microstructure of the IN718 and IN625 welds, respectively, in the heat-treated condition. In

both cases, again, EBSD inverse pole figure maps in three perpendicular directions, as well as the corresponding inverse pole figures, are given. Here, also, the building direction is parallel to the horizontal direction. The inverse pole figures were also determined for the entire area of the EBSD maps and, accordingly, indicate the crystallographic preferential orientations for all zones (BM, HAZ, WZ). The heat treatment is observed to have a clear

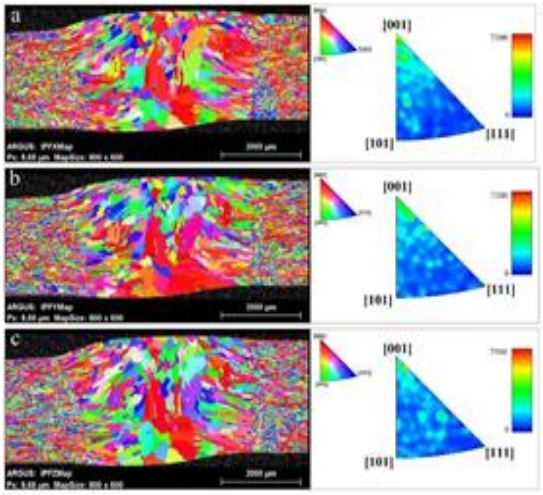

Figure 8. EBSD measurements on cross section IN718 with solution annealing heat treatment.

a) IPFX Map with inverse pole figure of X direction; b) IPFY Map with inverse pole figure of Y direction; c) IPFZ Map with inverse pole figure of Z direction.

effect in the microstructure of the BM and the HAZ, whose textures become clearly weaker, especially in the case of the IN625 material, where, simultaneously, elongated grains are replaced by more equiaxed and irregularly shaped crystallites. The grain size within the WZ remains significantly larger than that of the HAZ and BM. Within the WZ the main difference observed is the partial replacement of the elongated grains at the uppermost layer of the IN718 weld by smaller and more equiaxed crystallites, endowed with random orientations. The mentioned elongated shape is, however, retained in the IN625 WZ. In summary, our data reveal that the heat treatment significantly affects the microstructure and the texture of the BM and HAZ zones and that its effect on the WZ is less noticeable.

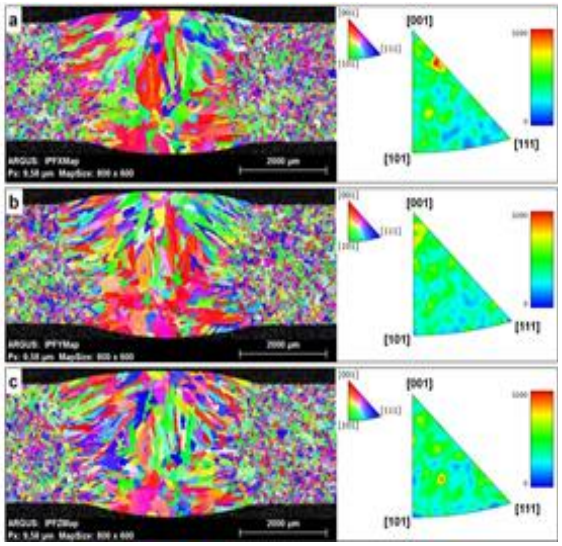

Figure 9. EBSD measurements on cross section IN625 with solution annealing heat treatment.

a) IPFX Map with inverse pole figure of X direction; b) IPFY Map with inverse pole figure of Y direction; c) IPFZ Map with inverse pole figure of Z direction.

The observed weakening of the texture of the BM and HAZ zones, which is more pronounced in the IN625 alloy, may be attributed to the occurrence of discontinuous recrystallization. This process consists of the long-range migration of high angle boundaries, thus facilitating the nucleation and growth of strain free grains with orientations that are different from those present in the as-built material. Partial discontinuous recrystallization is also the micro mechanism that leads to the appearance of randomly oriented grains at the uppermost layer of the IN718 weld. The feasibility of recrystallization

during post-processing heat treatments in SLM processed materials is highly dependent on the amount of strain energy stored during fabrication, which varies with process parameters and material types. Earlier works have demonstrated the occurrence of recrystallization in IN718 and IN625 samples fabricated by L-PBF processes following a solution treatment at similar temperature and holding time as those utilized in the present study, reported a degree of recrystallization of about 50 percent. Others have confirmed the presence of recrystallized grains when the solution treatment temperature exceeds 940 ˚C. Furthermore, they report that when the solution annealing temperature is increased to 980 ˚C, many recrystallized grains appear at the boundaries of laser scanning tracks and, consequently, the latter become faintly visible. This is consistent with the absence of melt pool traces in the BM and HAZ of the heat-treated samples of the present study (Fig. 7), in which the solution temperatures were 1175˚C for IN718 and 980˚C for IN625. Additionally, Li et al. report that recrystallized grains in L-PBF processed, and solution treated IN625 have random orientations. The microstructural evolution of the BM and HAZ of the Ni superalloys investigated here are fully consistent with earlier works.

The absence of significant microstructural evolution upon heat treatment within the WZ of the investigated materials is consistent with the presence in these zones of lower levels of stored energy because of grain growth during welding, resulting in a smaller driving force for recrystallizations. The observed lack of significant microstructural change reveals, instead, that only recovery processes, which are not detectable in the EBSD maps provided here as they involved only dislocation rearrangement processes.

The local variation of the Vickers hardness was evaluated in the Ni-superalloy welds, both in the as-built and heat-treated conditions. The cross area of the welds was segmented for hardness evaluation as indicated in the upper part of Fig. 10. The corresponding HV-values are given also in the same figure.

In summary, this study demonstrates the weldability of both Ni superalloys using the TIG method. A weld parameter variation outside of the standard parameters is thus not needed. Both, IN718 and IN625, can be TIG-welded using the same welding parameters and materials. Visually no major defects could be seen on any weld seam, regardless of the material and heat treatment. Although no local hardness peaks were found in any of the

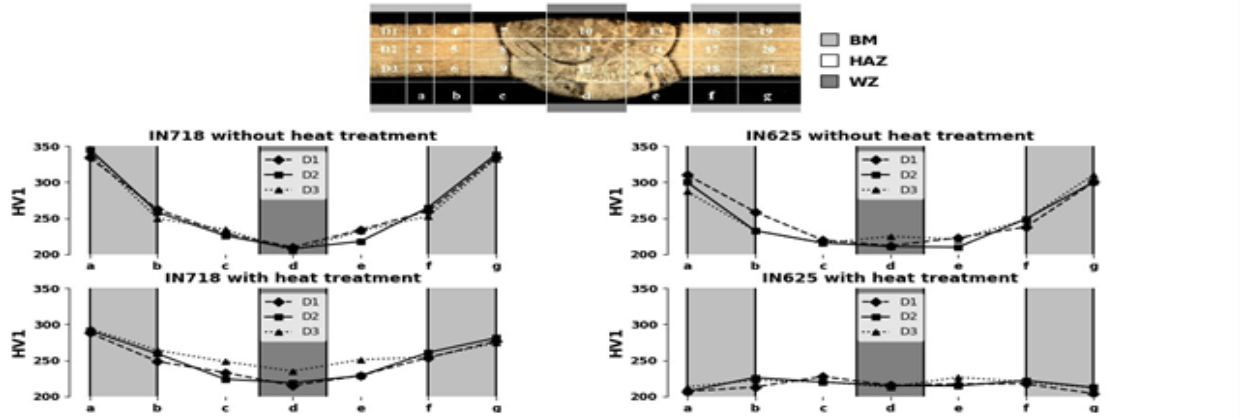

Figure 10. Top: Hardness measurement locations, Bottom: Vickers Hardness at the cross sections of IN625 and IN718 with and without heat treatment.

specimens, the as-built IN718 exhibits hardness values close to the permissible limit of 375 HV in the BM. Hence, a heat treatment before or after welding is not necessary, but still recommended. This is consistent with the fact, that the IN718 is used in its γ'' hardened form in most cases, meaning that the production setup without any heat treatment has no relevance in the industry today. The near-surface porosity in all specimens is thought to be caused by a suboptimal contour scanning strategy, which has been addressed in new parameter developments thereafter.

4. Conclusions

The weldability of L-PBF manufactured pipes made of IN718 and IN625 using TIG welding has been demonstrated in this study. No defects or weak points, which would preclude a process qualification according to industry standards, have been discovered. Both materials are applicable for production by laser powder-bed fusion and subsequent tungsten inert gas welding. The results show that heat treatment is not necessary for a positive welding result. However, heat treatment is recommended for IN718. Based on the results of this study, a full qualification of a process chain involving TIG welding of L-PBF manufactured parts into bigger assemblies is to be expected. This study is an early step toward integrating the L-PBF technology into mass production chain process. Further research is required to fully industrialize the technology. For future studies, we recommend investigations on the mechanical properties of TIG-welded tensile test bars produced by L-PBF. Additionally, welding tests combining L-PBF with wrought or cast materials can be interesting for certain use cases and should be carried out as described in this study.

5. APPLICATION

The adoption of AM parts in AFVs is new in comparison to other commercial industries. Some limited use cases have been publicized previously for small format, specialty applications. Siemens Energy has partnered with BAE Systems to develop a series of additively manufactured airflow ducts to improve cooling performance on their M88 Recovery Vehicle for the United States Army shown below.

Vehicles of this type make substantial use of structural steel and aluminum castings. It has been found that many such components are candidates for production by additive manufacturing utilizing welded Inconel 625 or 718 sub-assemblies. As a result of these material substitutions, collaboration between system integrators and sub-component engineers early in the development cycle helps to ensure effective product design. This allows designers to take advantage of higher material properties of nickel-based materials to reduce the cost and performance differences between the existing part and a new, additive design.

At current, focus has been on the development of high-performance components in sub-assemblies where specific requirements or constraints makes conventional manufacturing approaches difficult, impractical, or impossible. In these instances, it has been found that welded components whose sub-parts are printed from Inconel 625

offer substantial performance benefits. Drawbacks are that high performance components such as this come at a premium in cost. An additional benefit to the use of AM in this new generation of components, is that by designing welded features into the build-model, machining steps can be reduced and the potential for damaging components during weld preparation are reduced. Features such as weld joint preparation (groove or fillet) and timing features (for locating sub-components) can be added during the print and joined successfully with minimal additional preparation.

The technological and manufacturing readiness of nickel-based additive manufacturing technologies are mature in several industries including energy generation. As a result, this makes the use of AM, Inconel 625 weldments attractive for use on AFVs. Current needs in this area are better understanding of the processing, properties, and resultant component performance as relevant to Army ground systems as they are widely established in other applications. Additional studies on cost reduction, effective design & implementation of components in this application, and on-vehicle performance should be developed.

Acknowledgments: The authors would also like to express their sincere gratitude to the whole team of the metallurgical laboratory at Siemens Energy in Berlin; especially, but not limited to: Prof. Dr. Andreas Neidel, Carsten Geisler, Erhan Cagliyan, Boromir Fischer and Susanne Riesenbeck.

Abbreviations

The following abbreviations are used in this document:

AM	Additive Manufacturing
L-PBF	Laser Powder-Bed Fusion
IN718	Inconel 718
IN625	Inconel 625
TIG	Tungsten Inert Gas
HAZ	Heat Affected Zone
BM	Base Material
WZ	Weld Zone
EBSD	Electron Backscatter Diffraction
IPF	Inverse Pole Figure
HV	Vickers Hardness
NDT	Non-Destructive Testing